Journal of
Holography and Speckle
Vol. xx, 1–13, 2009

Holographic Optical Beam Combining, Splitting and Cross-Coupling: Numerical Analysis and Experimental Investigation

H. N. Yum[1], P. R. Hemmer[1], Renu Tripathi[2,*], and M. S. Shahriar[3]

[1] *Department of Electrical Engineering, Texas A&M University, College Station, Texas 77843, USA*
[2] *Department of Physics and Pre-Engineering, and Center for Research and Education in Optical Sciences and Applications, Delaware State University, Dover DE 19901, USA*
[3] *Department of Electrical Engineering and Computer Science, Northwestern University, Evanston IL 60208, USA*

In this paper, we present the coupled-wave analysis for multiple thick holographic gratings for optical beam combining. Starting with the basic model of incoherently superimposed multiple gratings used to form the beam-combiner, we derive equations that describe wave propagation in a holographic substrate containing angular multiplexed gratings with either sinusoidal refractive index or absorption modulation including the off-Bragg matched condition. Numerical results are presented for multiple thick holographic gratings in three different geometries: the beam-splitter mode, the beam-combiner mode, and the cross-coupled mode. The effect of non-equal beam intensities and phased angle variation on the efficiency of beam combiner have been investigated. Experiment is performed to create an efficient six beam splitter-combiner using a thick photopolymer based holographic material. The experimental measurement for efficiency in beam combining compares well with the predicted value from our theoretical model.

Keywords:

RESEARCH ARTICLE

1. INTRODUCTION

Various industrial and technological fields require cost effective and efficient ways to create high power lasers. An efficient incoherent beam-combiner could be very useful to generate high power laser beams[1–4] from multiple low power sources. One useful method to combine beam is a holographic beam combiner[5–7] with incoherently superimposed index gratings recorded in a holographic media. This is a very simple, cost-effective and efficient method. The only constraint of a holographic beam combiner is the diffraction efficiency of multiple gratings recorded on the holographic material, and the cross-talk among the gratings.

In a previous paper,[6] we demonstrated a coherent holographic beam combiner (CHBC). We recorded six superimposed holographic gratings with a reference wave at a fixed incident angle and six objective waves at different incident angles. In the beam splitter mode, the beam profiles for transmitted and diffracted waves were monitored and were compared with numerical simulations to determine the strengths of the 6 gratings. In the reverse mode, we demonstrated combination of six beams into a single beam, by controlling the relative phases between the six beams. The quality of the CHBC for the six beams was evaluated by comparing the experimental data with numerical simulations.

In this paper, we extend the previous study which was mainly focused on the beam combiner mode, and present a complete theoretical analysis along with simulation results for a holographic beam combiner which could act as a beam splitter and a cross-coupler in alternate geometries. We have used the coupled-wave theory to describe an angle-multiplexed multiple-grating holographic medium as an efficient optical element for beam combining, splitting and cross-coupling. The grating modulation strength for optimum performance in each mode of its operation is determined by numerically solving coupled-wave equations for a holographic substrate with N-multiplexed gratings. The analysis is restricted to thick index gratings in a lossless medium under Bragg matched condition. Our numerical results show that 100% conversion is achievable for each of these modes. Effect of non-equal beam intensities and phase angle variation between adjacent waves

*Author to whom correspondence should be addressed.

on beam combining have been studied using numerical examples. A thick photopolymer based holographic material is used in our experiment to create an efficient beam combiner using angle multiplexing. The grating strength is measured from the experimentally observed beam profiles using a single exposure technique recently proposed by us for the M# measurement.[8] Grating modulation close to the maximum diffraction efficiency condition has been achieved experimentally for six multiplexed gratings on a holographic substrate to demonstrate an efficient beam combining. In what follows, we review the coupled-wave theory and present an analysis for multi-wave mixing in a thick holographic medium in the context of beam combining, splitting and cross-coupling.

Diffraction efficiency of a thick hologram and the amplitudes of signal and reference waves can be obtained from the coupled wave theory[9] for thick hologram gratings. Thick holographic gratings cause energy exchange between the incoming reference wave and the outgoing signal wave at or near the Bragg angle. The analysis of the Bragg-matched diffraction for two sets of incoherently superimposed gratings using coupled wave theory was later developed by Case.[10] He determined the efficiencies of the diffracted waves for an index-modulated lossless holographic material and experimentally demonstrated two different modes of operation such as the beam splitter and combiner. Magnusson[11] considered the first and higher diffracted orders in gratings with arbitrary shapes and all possible incident angles including the Bragg angle. Furthermore, equations for efficiencies of higher order diffracted beams, which can be significant in holographic gratings with large refractive index modulations ($n_1 \approx 10^{-3} \sim 10^{-1}$), were obtained by using the coupled wave analysis. A different approach to analyze diffraction from two incoherently superimposed gratings was investigated by Zhao et al.[12, 13] They described a volume-index grating vector and examined the Bragg matching and pseudo phase matching cases. Kobolla[14] also investigated a beam splitter with multiple gratings recorded sequentially by one reference wave and object waves in a lossless holographic material and under the Bragg-matched condition.

We consider a general number of gratings recorded by one reference wave and multiple object waves. The incident angle of the reference wave is unchanged, while the object waves with a varying incident angle for each sequential exposure interfere with the reference wave. We then calculated the diffraction efficiency for the cases (i) an incoming wave in the direction of the reference wave, (ii) several input waves with equal intensities propagating in the direction of the object waves. Diffraction efficiency for the incoming waves with non-equal intensities is also studied. In our experiment, six gratings are recorded by angular multiplexing which is considered as a six beam combiner. In order to predict the efficiency of the beam combiner, grating strength is evaluated by comparing the experimental results to our simulation in the beam splitter mode. The six beam combiner is demonstrated using a simple set-up with a plano-convex lens and a mirror.

2. COUPLED-WAVE ANALYSIS FOR MULTIPLE THICK HOLOGRAPHIC GRATINGS

We derive equations that describe wave propagation in angular multiplexed grating structure with a sinusoidal refractive index (or absorption) modulation including the off-Bragg matched condition. We consider multiple incoherently superimposed gratings for our designs of beam combiner, beams splitter and beam coupler. Figure 1 shows the basic diagram of the thick grating model used in our analysis.

For simplicity, we assume that the gratings are recorded in an optical material, which is infinite in extent along the x and y direction, and all the waves are propagating in the x–z plane, and polarized in the y direction. The grating is defined by the grating vector $\mathbf{K_h}$ and its length is $K_h = 2\pi/\Lambda_h$, where Λ_h is the period of the hth multiplexed grating.

When the wave is polarized perpendicular to the plane of incidence, wave propagation in presence of multiple gratings can be described in terms of the scalar wave equation as

$$\nabla^2 E(x,z) + k^2 E(x,z) = 0 \tag{1}$$

where $E(x,z)$ is the complex amplitude distribution, assumed to be independent of y. Material modulations constituting the holographic gratings can be expressed by

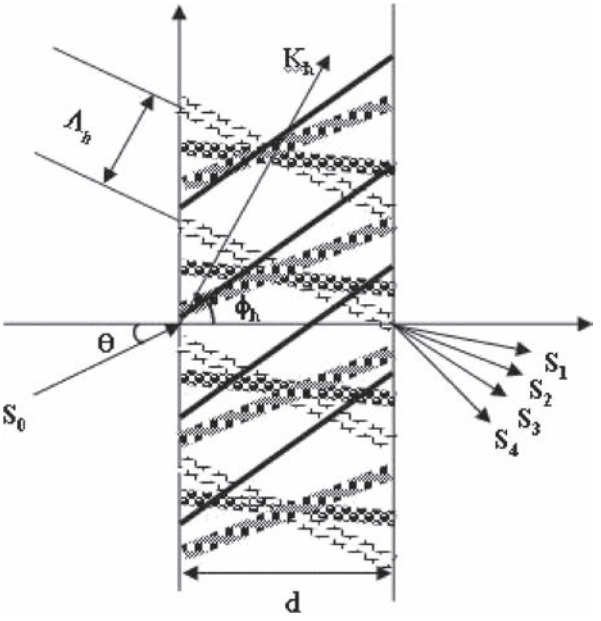

Fig. 1. Schematic illustration of the reconstruction of object waves from the superimposed multiple holographic gratings illuminated by a reference wave.

either the spatial variations of the relative dielectric constant ε, or the conductivity σ. If ε_h and σ_h are the amplitudes of the spatial modulations of the hth grating, the modulated quantities of ε and σ can be written as

$$\begin{aligned}\varepsilon &= \varepsilon_0 + \textstyle\sum_{h=1}^{N} \varepsilon_h \cos(\mathbf{K_h}\cdot\mathbf{X}) \\ \sigma &= \sigma_0 + \textstyle\sum_{h=1}^{N} \sigma_h \cos(\mathbf{K_h}\cdot\mathbf{X})\end{aligned} \tag{2}$$

where ε_0 is the average dielectric constant,σ_0 the average conductivity and $\boldsymbol{X} = (x, y, z)$. This results in a spatially modulated propagation constant k

$$k^2 = \frac{\omega^2}{c^2}\varepsilon - j\omega\mu\sigma \tag{3}$$

where c is the light velocity in free space and μ is the permeability of the material. Inserting Eq. (2) into Eq. (3), we obtain

$$k^2 = \beta^2 - 2j\alpha\beta + \sum_{h=1}^{N} 2\beta\kappa_h(e^{-j\mathbf{K_h}\cdot\mathbf{X}} + e^{j\mathbf{K_h}\cdot\mathbf{X}}) \tag{4}$$

where

$$\beta = \frac{\omega}{c}\sqrt{\varepsilon_0}, \text{ and } \alpha = \frac{\mu c\sigma_0}{2\sqrt{\varepsilon_0}} \tag{5}$$

and the coupling constant κ_h between the reference wave S_0 and the hth diffracted wave S_h from the hth grating is

$$\kappa_h = \frac{\pi n_h}{\lambda} - j\frac{\alpha_h}{2}; \quad n_h = \frac{\varepsilon_h}{2\sqrt{\varepsilon_0}}; \quad \alpha_h = \frac{c\mu\sigma_h}{2\sqrt{\varepsilon_0}} \tag{6}$$

where n_h and α_h are the spatial modulation amplitudes of the refractive index and the absorption constant. The diffracted waves and the reference wave have the propagation vectors ρ_h and ρ_0, respectively that satisfy the following phase matching relation

$$\boldsymbol{\rho}_h = \boldsymbol{\rho}_0 - \mathbf{K_h} \tag{7}$$

The components of $\boldsymbol{\rho}_0$ and $\mathbf{K_h}$ are given by

$$\boldsymbol{\rho}_0 = \beta\begin{bmatrix}\sin\theta \\ 0 \\ \cos\theta\end{bmatrix}, \quad \mathbf{K_h} = K_h\begin{bmatrix}\sin\phi_h \\ 0 \\ \cos\phi_h\end{bmatrix} \tag{8}$$

At the Bragg angle, $\theta_{h_{\text{Bragg}}}$ of the hth grating

$$\beta^2 - \boldsymbol{\rho}_h^2 = 0 \tag{9}$$

Combining Eqs. (7) and (8), and using the Eq. (9), one obtains

$$\cos(\phi_h - \theta_{h_{\text{Bragg}}}) = K_h/2\beta \tag{10}$$

We describe the waves in the medium (Fig. 1) with complex amplitudes S_0 and S_h that vary along z. The total electric field incident on the gratings can be written as

$$E = S_0(z)e^{-j\rho_0\cdot\mathbf{x}} + \sum_{h=1}^{N} S_h(z)e^{-j\rho_h\cdot\mathbf{x}} \tag{11}$$

By using Eqs. (4) and (11) in (1), we obtain

$$\begin{aligned}&\left(S_0'' - 2jS_0'\rho_{0z} + (\beta^2 - \rho_0^2)S_0 - 2j\alpha\beta S_0 + 2\beta\sum_{h=1}^{N}\kappa_h S_h\right)e^{-j\rho_0\cdot\mathbf{x}} \\ &+ \sum_{h=1}^{N}\big((S_h'' - 2jS_h'\rho_{0z} + (\beta^2 - \rho_h^2)S_h \\ &\qquad -2j\alpha\beta S_h + 2\beta\kappa_h S_0)e^{-j\rho_h\cdot x}\big) = 0\end{aligned} \tag{12}$$

where the primes indicate spatial derivatives of the field amplitudes in the z direction. The propagation vector $\boldsymbol{\rho}_0$ of the reference wave S_0 is equal to the wave propagation vector in the absence of the gratings, i.e., $\beta^2 - \rho_0^2 = 0$. We assume that the energy exchange between the diffracted orders is slowly varying. Consequently, the second order differential terms can be neglected. One can define the obliquity factors C_0, C_h and dephasing factor ϑ_h for the hth grating as

$$C_0 = \frac{\rho_{0z}}{\beta}, \quad C_h = \frac{\rho_{hz}}{\beta}, \quad \vartheta_h = \frac{\beta^2 - \rho_h^2}{2\beta} \tag{13}$$

where ρ_{0z} and ρ_{hz} are the z-components of ρ_0 and ρ_h respectively. By substituting Eq. (13) in Eq. (12), one can obtain the following equations for the amplitudes of diffracted and transmitted waves corresponding to N superimposed gratings

$$\begin{aligned}C_0 S_0' + \alpha S_0 &= -j\textstyle\sum_{h=1}^{N}\kappa_h S_h \\ C_h S_h' + (\alpha + j\vartheta_h)S_h &= -j\kappa_h S_0\end{aligned} \tag{14}$$

These coupled-wave equations are solved numerically for multiple thick gratings to describe three different modes of operation as beam-splitter, beam-combiner, and cross-coupler.

3. SIMULATION RESULTS FOR MULTIPLE BRAGG GRATINGS IN THREE DIFFERENT MODES

In the common-Bragg-angle structure with N incoherently superimposed gratings, the reference wave is common to every exposure so that the N gratings have the common Bragg angle ($\theta_{1_{\text{Bragg}}} = \theta_{2_{\text{Bragg}}} = \cdots\cdots\cdots = \theta_{N_{\text{Bragg}}} = \theta_{\text{Bragg}}$) and the readout wave has the same wavelength as that used for recording. There are three different modes in which the common-Bragg-angle structure can be read out:[9]

(i) The beam-splitter mode, where the structure is illuminated with the reference wave at the common Bragg angle. In this case, a single input wave reconstructs N object waves.

(ii) The beam-combiner mode is the time-reversal case of the first one. In this case, the N object waves illuminate the structure at the respective Bragg angles and thus, reconstruct the reference wave.

(iii) The cross-coupled mode, where the structure is illuminated with waves propagating in the direction of randomly picked object waves. For this mode, the input waves are initially diffracted into the direction of the reference wave. Successively, the reconstructed reference wave diffracts again into the directions of other object waves before leaving the grating structure.

We have investigated the efficiencies of the output waves for all the above three cases. It is assumed that a holographic material has N lossless dielectric gratings ($\alpha = 0$) and the Bragg-matched condition ($\vartheta_h = 0$) is satisfied. Using these assumptions, Eq. (14) can be written as

$$\begin{aligned} C_0 \mathrm{S}_0' &= -j \textstyle\sum_{h=1}^{6} \kappa_h \mathrm{S}_h \\ C_h \mathrm{S}_h' &= -j\kappa_h \mathrm{S}_0 \end{aligned} \tag{15}$$

The efficiency of the output wave S_h is defined as[9]s

$$\eta_h = \frac{|\, C_h \,|}{C_0} \mathrm{S}_h \mathrm{S}_h^* \tag{16}$$

Equations (7) and (8) give the z component of the propagation vector of the object wave for the hth grating. Inserting it in Eq. (13), the oblique factors C_0 and C_h, and the dephasing measure ϑ_h for the common Bragg angle structure in the Bragg matched condition can be obtained as

$$C_0 = \frac{\cos\theta_{\mathrm{Bragg}}}{\beta}, \quad C_h = \cos\theta_{\mathrm{Bragg}} - \frac{K_h \cos\phi_h}{\beta}, \quad \vartheta_h = 0 \tag{17}$$

where θ_{Bragg} is the common-Bragg-angle which is same as the incident angle of the reference wave.

The grating strength for a single hologram can be defined as

$$\nu = \frac{\pi n_1 d}{\lambda \sqrt{C_{\mathrm{R}} C_{\mathrm{O}}}} \tag{18}$$

where d is the thickness of a holographic material, C_{R} and C_{O} are the obliquity factors of reference and object wave respectively, and λ is wavelength of light. The grating strength ν_h for the hth grating is given by

$$\nu_h = \frac{\pi n_h d}{\lambda \sqrt{C_R C_h}} \tag{19}$$

We consider six recorded gratings in the medium and the grating strengths for all these gratings are considered equal ($\nu_1 = \nu_2 = \nu_3 = \nu_4 = \nu_5 = \nu_6 = \nu$). The diffraction efficiencies of the waves at $z = d$ for the three different configurations such as beam combiner, splitter and cross-coupler modes are plotted as a function of the equalized grating strength normalized by $\nu_0 = \pi/2$ in Figures 2, 3, 4, and 5. During the holographic recording, beam S_0 is used as a reference wave and the others $\mathrm{S}_1 \sim \mathrm{S}_6$ as objective waves. The common-Bragg-angle is $\pi/6$ and the first grating formed by the interfering beams S_0 and S_1 is nonslanted ($\phi_1 = \pi/2$). The gratings are recorded in a sequential order by interfering beams S_1 to S_6 with reference wave S_0. The angle difference between two object waves S_h and S_{h+1} is constant i.e., the six gratings are recorded using equal angular spacing. For the splitter mode, the boundary condition at $z = 0$ is

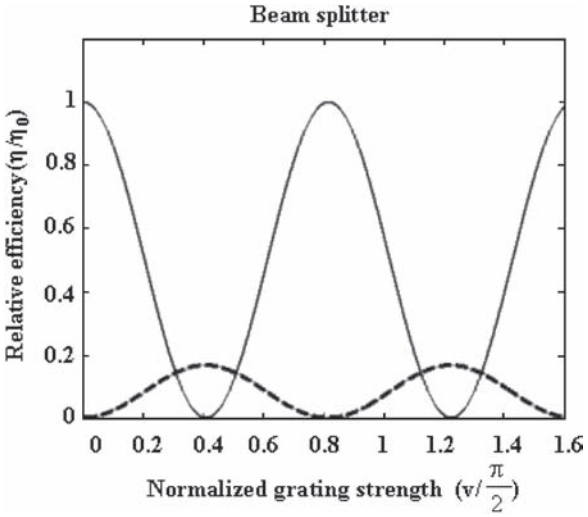

Fig. 2. Relative efficiencies η/η_0 for the holographic beam splitter as a function of grating strengths normalized with respect to $\nu_0 = \pi/2$, the grating strength which gives unit diffraction efficiency for a single hologram. — S_0, $\cdots$ $\mathrm{S}_1 \sim \mathrm{S}_6$.

$$\begin{aligned} \mathrm{S}_1(0) = \mathrm{S}_2(0) = \mathrm{S}_3(0) = \mathrm{S}_4(0) = \mathrm{S}_5(0) \\ = \mathrm{S}_6(0) = 0, \quad \mathrm{S}_0(0) = 1 \end{aligned} \tag{20}$$

where $\mathrm{S}_0(z)$ is the amplitude of the reference wave and $\mathrm{S}_1(z) \sim \mathrm{S}_6(z)$ are the amplitudes of the six object waves. The beam splitter divides the incident wave S_0 into the six waves with equalized maximum diffraction efficiencies when the equalized grating strength ν is $0.204\pi \cong \frac{1}{\sqrt{6}}\frac{\pi}{2}$ as shown Figure 2. The simulation result shows that

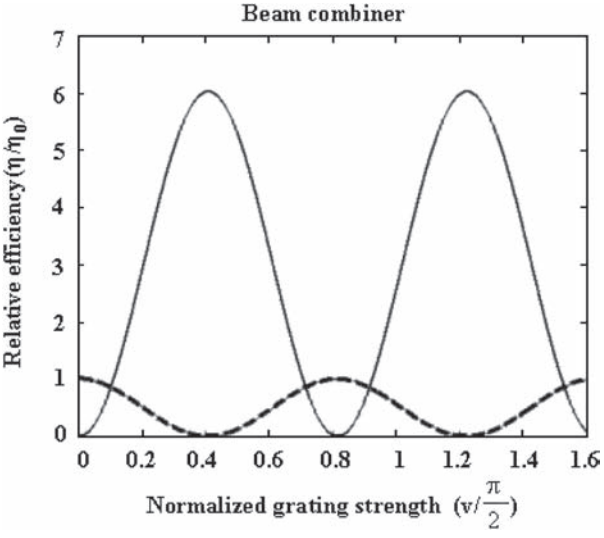

Fig. 3. Relative efficiencies η/η_0 for the holographic beam combiner. All input beams are assumed to be initially in phase. — S_0, $\cdots$ $\mathrm{S}_1 \sim \mathrm{S}_6$.

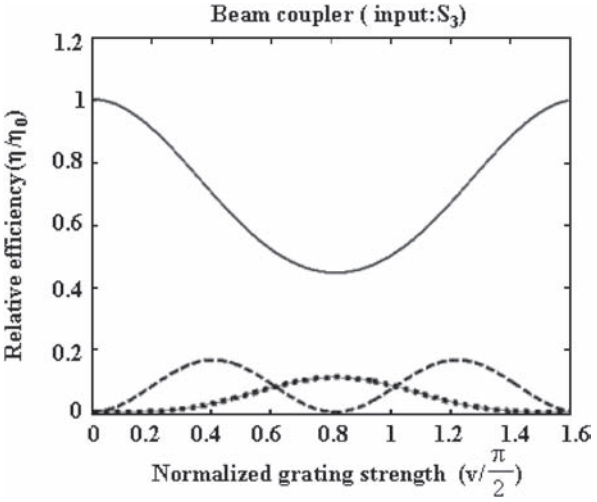

Fig. 4. Relative efficiencies η/η_0 for the cross-coupling plotted as a function of normalized grating strength. The input wave incident in the direction of the beam S_3 is illuminating the 6 multiplexed gratings. — S_3, ⋯ S_0, –■–■– S_1, S_2, S_4, S_5, S_6.

the output waves of the 1:6 beam splitter from S_1 to S_6 reach maximum diffraction efficiencies when all grating strengths are equalized to $\frac{1}{\sqrt{6}}\frac{\pi}{2}$. The result can be extended to the case of a beam splitter with N superimposed gratings that divides an incident wave into N partial waves with equalized maximum diffraction efficiency, when sum of the N grating strengths satisfy the equation[10, 14] $\left(\sum_{h=1}^{N}\nu_h^2\right)^{\frac{1}{2}} = \frac{\pi}{2}$.

For the beam combiner operation, the boundary condition is given by

$$\begin{aligned} S_1(0) = S_2(0) = S_3(0) = S_4(0) = S_5(0) \\ = S_6(0) = 1, \quad S_0(0) = 0 \end{aligned} \tag{21}$$

Since the beam-splitter acts as a beam-combiner in reverse, the beam combiner must show maximum efficiency at the same grating strength as when a beam splitter reaches the maximum diffraction efficiency. Figure 3 shows all input waves from S_1 to S_6 are fully combined and consequently the outgoing wave S_0 has the maximum efficiency when the individual grating strength is $\frac{1}{\sqrt{6}}\frac{\pi}{2}$.

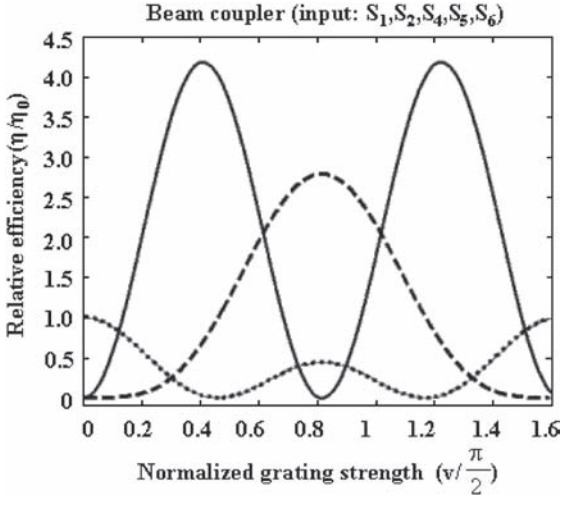

Fig. 5. Relative efficiency η/η_0 for the cross coupled mode. Five incident input waves S_1, S_2, S_4, S_5, S_6 are illuminating the six multiplexed gratings. — S_0, ⋯ S_3, –■–■– S_1, S_2, S_4, S_5, S_6.

For the cross-coupled mode, we considered two cases. In the first case, when an input wave is incoming along the direction of beam S_3, the efficiencies of outgoing waves are analyzed. The boundary conditions are

$$\begin{aligned} S_0(0) = S_1(0) = S_2(0) = S_4(0) = S_5(0) \\ = S_6(0) = 0, \quad S_3(0) = 1 \end{aligned} \tag{22}$$

As can be seen from Figure 4 that at the grating strength 0.4π, the input wave is diffracted into the direction of beam S_0 and the reconstructed wave in the direction of beam S_0 is completely diffracted into the five object waves S_1, S_2, S_4, S_5, S_6. The outgoing wave in the direction of beam S_0 disappears and the efficiencies show equalized maximum values in the directions of the five object waves. However, at the grating strength 0.2π, the reconstructed wave in the direction of beam S_0 can not be diffracted again into the five object waves before leaving a holographic material and the efficiency of the output wave in the direction of beam S_0 reaches maximum.

In the second case, we consider the reverse of the first of the first case. The five input waves are coming along the directions of the five object waves S_1, S_2, S_4, S_5, S_6 and the efficiencies of outgoing waves are analyzed. The boundary conditions are

$$\begin{aligned} S_0(0) = S_3(0) = 0, \quad S_1(0) = S_2(0) = S_4(0) \\ = S_5(0) = S_6(0) = 1 \end{aligned} \tag{23}$$

The efficiencies of outgoing waves are shown in Figure 5. At the grating strength 0.4π, five input waves produce a diffracted wave in the direction of beam S_0 and this diffracted wave is completely diffracted again into the direction of beam S_3 before leaving a holographic material. The outgoing wave in the direction of beam S_0 disappears and the efficiency of the output wave in the direction of beam S_3 shows maximum value. At the grating strength 0.2π, the five input waves are diffracted into the direction of beam S_0 and the reconstructed beam S_0 is partially diffracted again into the direction of beam S_3. However, the reconstructed beam is mostly outgoing, and efficiency of the outgoing wave in the direction of beam S_0 reaches maximum.

During the experiment, it is difficult to perfectly equalize the intensities of all the input waves. Therefore, we investigate the influence of non-equal input beam intensities on the efficiency of beam combiner so that we may predict the efficiency of the beam combiner for the real case. Efficiency of the output waves are plotted in Figures 6(a, b and c) for the case while non-equal amplitude waves are incident on the beam combiner. As shown,

a small amplitude variation of the input intensities causes a small loss in output intensity, resulting in output less than the sum of the square of amplitude for all the inputs. In Figure 6(a), for the case that the amplitude difference between adjacent inputs is 16% of the strongest input amplitude, the output intensity of S_0 is about 76% of the sum of the intensities. Thus in the worst case when the input amplitude difference is large, the output of S_0 shows only a 24% drop in efficiency. Figures 6(b) and (c) show the output is 90% and 98% of the sum of input intensity when the amplitude difference is 10% and 5% respectively. Therefore, the output loss caused by non-equal input waves is concluded to be very small if the intensities of input waves are adjusted within 5%.

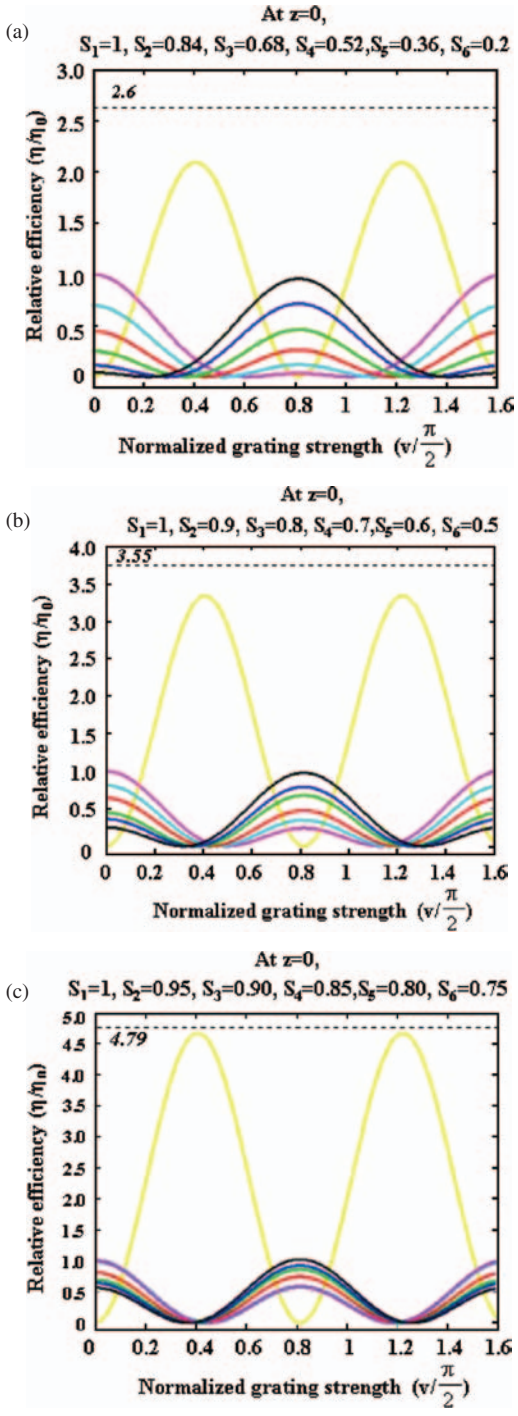

Fig. 6. Relative efficiency η/η_0 for the case of six non-equal intensities of the input beams in the beam combiner mode are plotted. Amplitude difference between adjacent inputs is set to three different values (a) 0.16, (b) 0.1, (c) 0.05. Yellow: S_0, Magenta: S_1, Cyan: S_2, Red: S_3, Green: S_4, Blue: S_5, Black: S_6.

Relative efficiency can be obtained by calculating square of the input amplitudes when normalized grating strength $v/(\pi/2)$ is set to a zero. However, there exists a difference in value between the relative efficiency obtained from the simple calculation and from numerical simulation shown in graphs above. Such discrepancy results from the ratio of the obliquity factors, $|C_h|/C_0$ in Eq. (16) which is considered in the numerical simulation, but not in the simple calculation.

4. DETERMINATION OF EQUALIZED GRATING STRENGTH BY ANALYZING THE OUTPUT WAVES IN THE BEAM SPLITTER MODE

In this section, we estimate equalized grating strength by analyzing the output waves when an input wave propagates along the direction of reference wave. The reference is diffracted by 6 gratings recorded using angular multiplexing. The images of the diffracted waves are compared to the graphs of numerical simulation which provides the intensities of output waves for an arbitrary equalized grating strength as a function of the beam radius.

The input wave S_0 illuminates N superimposed holograms with equalized gratings at the common Bragg angle and is diffracted into waves $S_1 \sim S_N$. The output waves $S_1 \sim S_N$ propagate along the direction of each object wave. The boundary conditions for Eq. (12) at $z = 0$ can be written as

$$S_0(0) = 1, \quad S_1(0) = S_2(0) = \cdots = S_N(0) = 0 \tag{24}$$

We are interested in the amplitudes of output waves at $z = d$. The solutions of the differential equations at $z = d$ are written as[5, 10]

$$\begin{aligned} S_0(d) &= \cos\left(\sqrt{\textstyle\sum_{h=1}^{N} \nu_h^2}\right) \\ S_k(d) &= -j\frac{\nu_h}{\sqrt{\sum_{h=1}^{N} \nu_h^2}} \sin\left(\sqrt{\sum_{h=1}^{N} \nu_h^2}\right) \end{aligned} \tag{25}$$

where v_h is the grating strength for the hth hologram.

Consider that the holograms are recorded using a Gaussian beam. The index modulation amplitude is then proportional to the intensity of the recording beam. The grating strengths of all recorded holograms are equal and

will show the Gaussian profile along the beam radius. The grating strengths for each hologram can be expressed as

$$\nu_h = \frac{\pi n_h d}{\lambda\sqrt{C_0 C_h}} = A\exp\left(-\frac{2r^2}{\varpi_0^2}\right), \quad (h = 1\sim N, v_1 = v_2 = \cdots = v_N = v) \tag{26}$$

where C_0 and C_h are the obliquity factors of S_0 and S_h respectively, n_h are the index modulation amplitudes, A is an equalized grating strength value at the center of the recording beam, and ω_0 is the Gaussian beam radius of the recording beam. Readout is performed at the same wavelength as that used for hologram recording. Combining Eqs. (25) and (26), S_0 and S_h can be written as

$$\begin{aligned} S_0(d) &= \cos\left(\sqrt{N}A\exp\left(-\tfrac{2r^2}{\varpi_0^2}\right)\right) \\ S_h(d) &= -j\frac{1}{\sqrt{N}}\sin\left(\sqrt{N}A\exp\left(-\frac{2r^2}{\varpi_0^2}\right)\right) \end{aligned} \tag{27}$$

Readout beam also shows the Gaussian profiles radially. Multiplying the Eq. (27) by a Gaussian envelope, the amplitude behavior of outgoing waves at $z = d$ in the radial direction can be expressed by

$$\begin{aligned} S_0(r) &= \cos\left(\sqrt{N}A\exp\left(-\tfrac{2r^2}{\varpi_0^2}\right)\right)\exp\left(-\tfrac{r^2}{\varpi_1^2}\right) \\ S_h(r) &= -j\frac{1}{\sqrt{N}}\sin\left(\sqrt{N}A\exp\left(-\frac{2r^2}{\varpi_0^2}\right)\right)\exp\left(-\frac{r^2}{\varpi_1^2}\right) \end{aligned} \tag{28}$$

where ω_1 is the Gaussian radius of the reading beam. From Eq. (28), it is noticed that when N superimposed holograms are considered as a single hologram, an effective accumulated grating strength for N holograms at the center of beam is $\sqrt{N}$ times the grating strength of an individual grating denoted as A. One can insert Eq. (28) into Eq. (16) and obtain the efficiency of the output wave as a function of r

$$\eta_h = \frac{|C_h|}{C_0} S_h(r) S_h*(r), \quad (h = 0\sim N) \tag{29}$$

where $S_h*(r)$ represents the conjugate of $S_h(r)$.

Figure 7 shows the combined experimental setup for the hologram writing and readout. The holograms are recorded using an Nd-YAG laser ($\lambda = 532$ nm) and the read-out is performed with the same laser used in recording. We recorded 4 holograms in the 1st sample and 6 holograms in the 2nd sample with different exposure schedule using angular multiplexing. In this set-up, the incident angle of the reference wave S_0 is fixed during every exposure. Therefore, a common Bragg angle can be established. During the readout, a beam illuminates the holograms at the common Bragg angle and the beams $S_1\sim S_N$ are reconstructed simultaneously under the Bragg matched condition. Angle displacement between adjacent object waves is constant. The holographic material with 4 holograms was baked for 3 hours and that with 6 holograms for 2 hours. We compared observed experimental images with simulation results from optional A values and evaluated the optimized A value which makes efficiency profiles identical to the experimentally observed images of output waves.

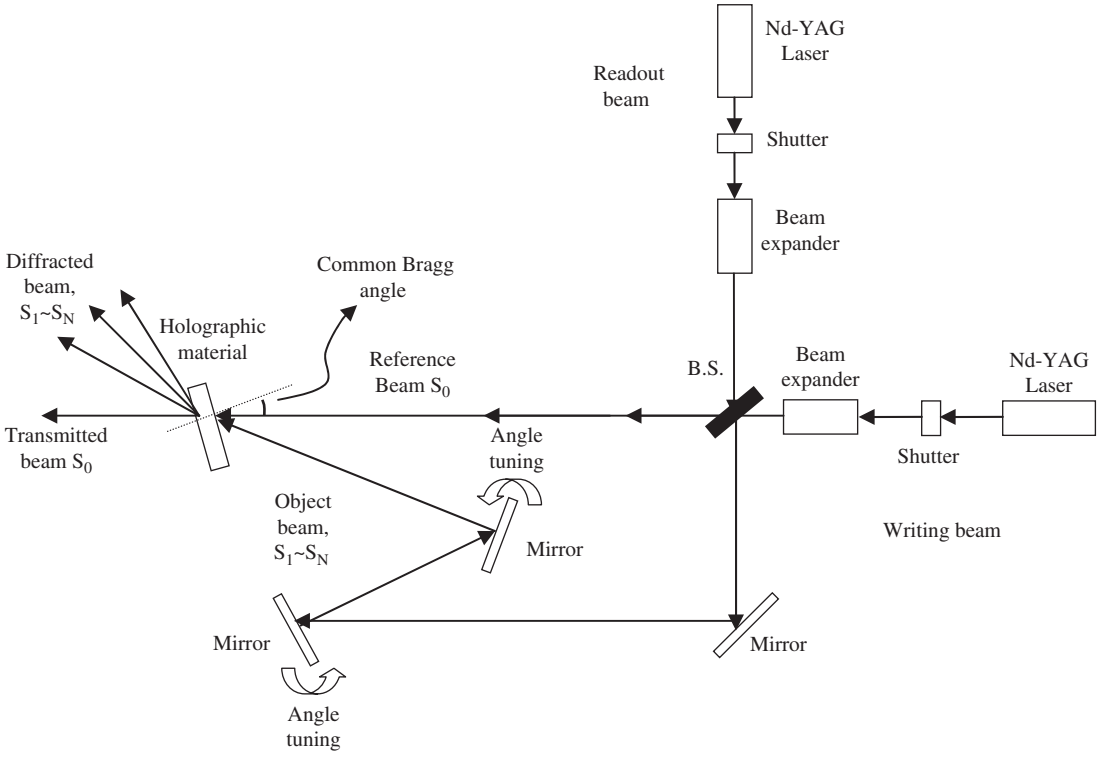

Fig. 7. Recording set-up for angular multiplexing using the Nd-YAG laser. The read-out is performed using another Nd:YAG laser.

Table I. Experimentally observed transmitted and diffracted patterns for 4 superimposed gratings. The profiles show the relative efficiency η/η_0, as a function of the beam radius. The unit of beam radius along the x-axis is in "μm" and the peak efficiency η_0 is normalized to unity.

A = 1.08π	Exposure time (sec)	Images	Profiles
S_0		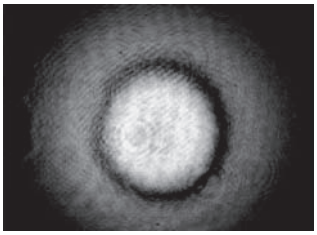	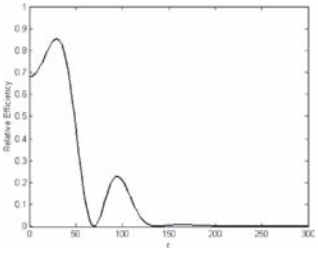
S_1	13	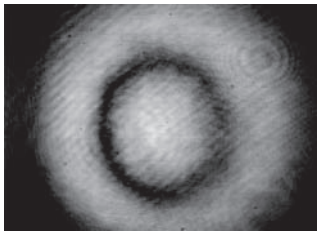	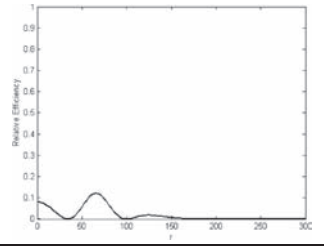
S_2	13	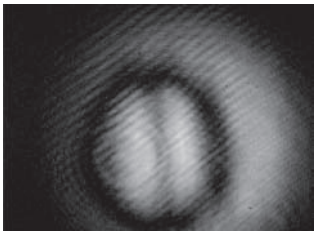	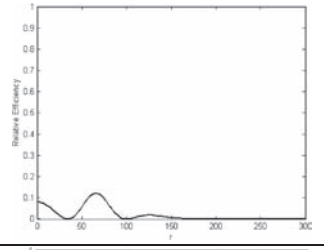
S_3	17	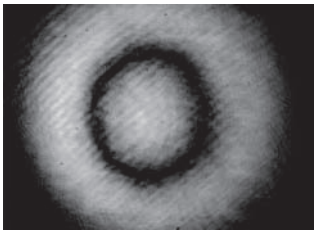	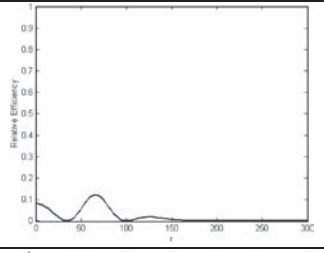
S_4	21	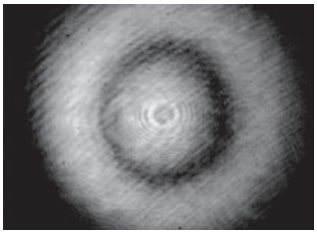	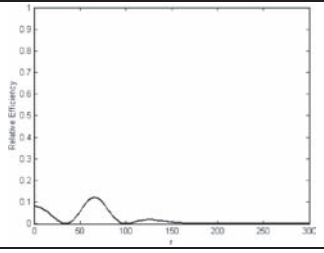

Tables I, II show the transmitted and diffracted images of 4 and 6 superimposed holograms, and the exposure schedules used. In Table I, the diffraction image of S_2 shows low efficiency as compared with that of S_1, S_3, S_4 and a fringe in the bright region is observed inside the ring possibly because of the mode hopping of the laser during the 2nd exposure. By comparing the number of rings observed in the images with the profiles, one can also determine the equalized grating strength of 4 holograms to be 1.08π. In Table II, it is also determined that the equalized grating strength of the 6 holograms reached a value of 0.23π. It is higher than $0.204\pi(\approx \frac{\pi}{2\sqrt{6}})$, the value at which the simulated beam splitter was shown to have the maximum diffraction efficiency. The sample adequately functions as a high efficiency beam splitter. If used in reverse, it can also function as a high efficiency beam combiner based on our discussions before.

Table III shows the intensities of the transmitted wave, S_0 and diffracted waves $S_1 \sim S_6$ measured using the 2nd sample shown in Table II. The output intensity data in Table III indicates that the input beam is diffracted into 6 beams with the almost equalized intensity. As mentioned earlier, the equalized grating value is measured to be 0.23π which deviates slightly from the optimum value

Table II. Experimentally observed transmitted and diffracted patterns for 6 superimposed gratings.

A = 0.23π	Exposure time (sec)	Images	Profiles
S_0		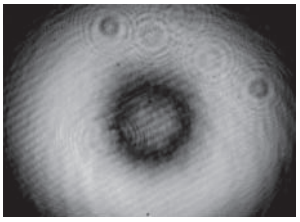	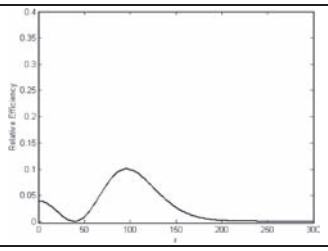
S_1	4	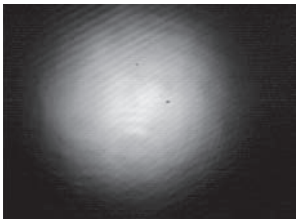	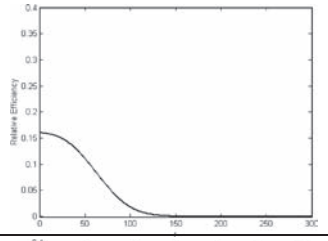
S_2	3.5	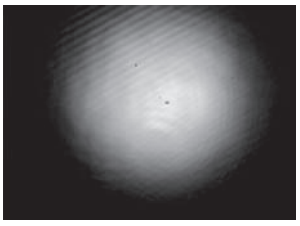	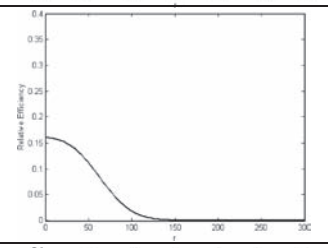
S_3	3.5	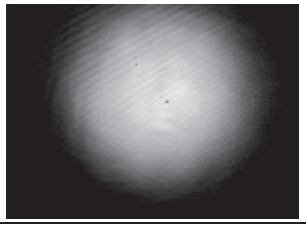	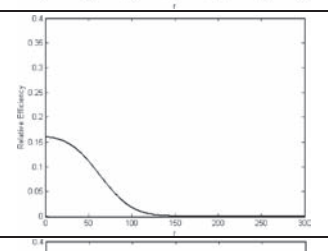
S_4	3.2	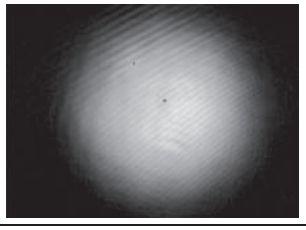	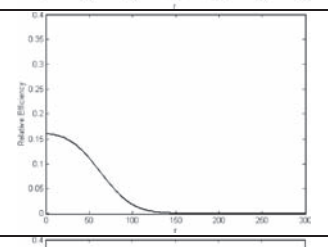
S_5	3.2	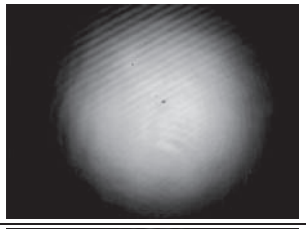	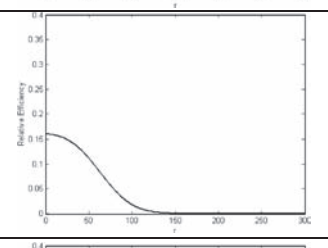
S_6	3.2	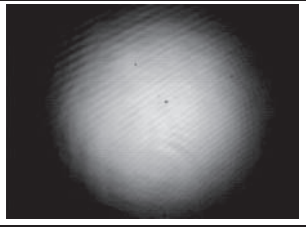	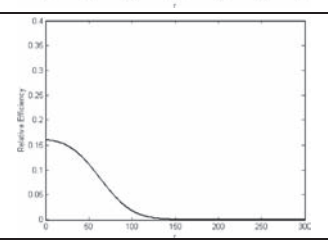

Table III. Intensities of the transmitted and diffracted waves measured in experiment using the 2nd sample shown in Table II.

	S_0	S_1	S_2	S_3	S_4	S_5	S_6
Power intensity (V)	0.1	0.5	0.53	0.32	0.5	0.44	0.34

0.204π. However it clearly demonstrates a near maximum diffraction efficiency 6 beam splitter.

5. INFLUENCE OF PHASE ANGLE VARIATION BETWEEN THE INPUT WAVES ON THE INTENSITY OF AN OUTPUT WAVE

An output of a six beam combiner is investigated using a numerical simulation based on the assumption that at the entrance of a holographic material, phase difference exists between each input wave. We also imposed the additional condition that the phase angle difference between adjacent input waves is constant. Therefore, the boundary conditions at $z = 0$ are

$$S_0(0) = 0, \quad S_1(0) = 1, S_2(0) = e^{j\phi}, S_3(0) = e^{j2\phi}, \\ S_4(0) = e^{j3\phi}, \ldots S_N(0) = e^{j(N-1)\phi} \tag{30}$$

where ϕ is the phase difference between adjacent waves. We obtain the solution of the amplitude of S_0 at $z = d$

$$S_0(d) = -\frac{1}{2}\sqrt{\frac{\prod_{h=1}^{N} C_h}{C_0\gamma}}\left[\sum_{h=1}^{N}\kappa_h e^{j(h-1)\phi}\right] \\ \times\left[\exp\left(j\sqrt{\frac{\gamma}{\prod_{h=0}^{N} C_h}}d\right) - \exp\left(-j\sqrt{\frac{\gamma}{\prod_{h=0}^{N} C_h}}d\right)\right] \tag{31}$$

with $\gamma = \sum_{h=1}^{N}\left[\frac{\left(\prod_{k=1}^{N} C_k\right)\kappa_h^2}{C_h}\right]$

The intensity of the output wave, I can be written as

$$I = S_0(d)S_0*(d) \tag{32}$$

In our analysis for the intensity profiles of output wave, it is assumed that the grating strengths for N holograms are equalized to the value at which beam combiner shows maximum diffraction efficiency. This assumption yields the equalized grating strength for N superimposed holograms as $\nu_1 = \nu_2 = \nu_3 = \cdots\cdots\cdots = \nu_{N-1} = \nu_N = \nu = \pi/2\sqrt{N}$. The beam intensities from Eq. (32) are plotted as a function of phase difference ϕ between adjacent input waves in Figures 8(a), (b), (c) for three cases considering 3, 6, and 9 incoming waves and the grating strengths are equalized to the value of $\pi/2\sqrt{N}$. In the three cases, in-phase input waves are completely combined and the intensities reach maximum value which is equal to the sum of the intensity of individual input waves. Figures 8(a),

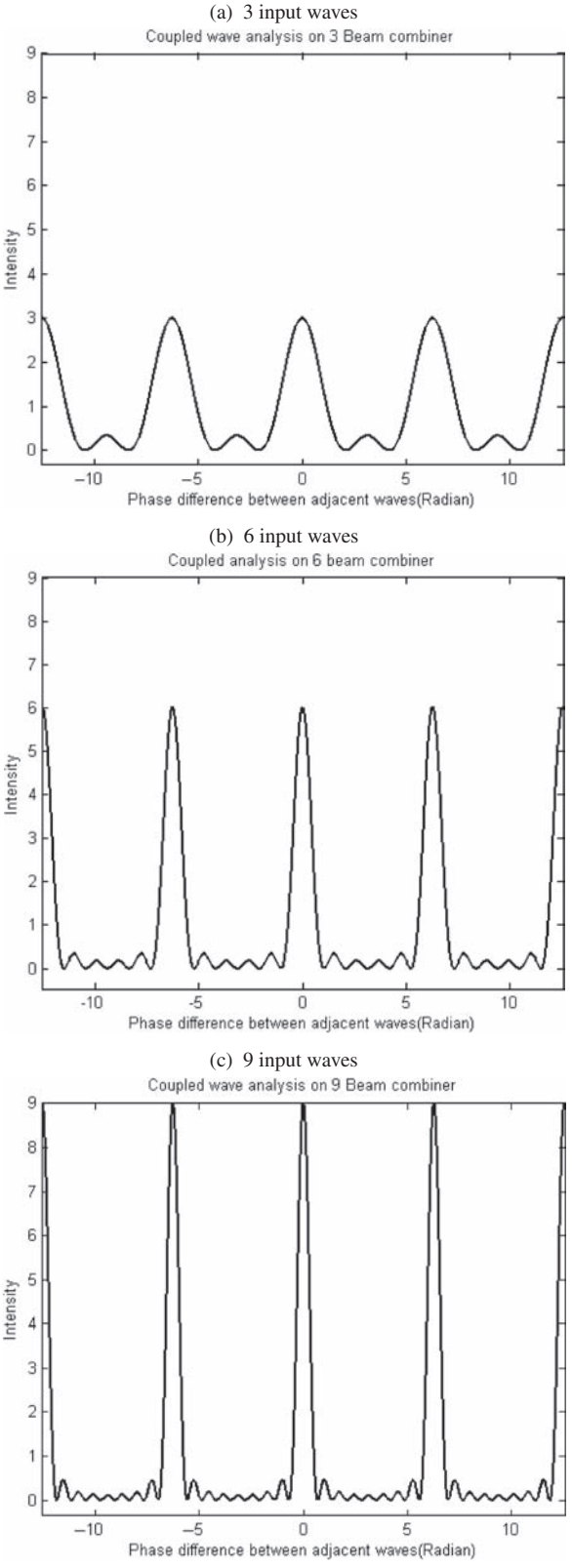

Fig. 8. Calculated intensity of the output wave in the direction of reference wave S_0 as a function of the phase angle between the adjacent input waves. Every input wave is considered to have unit intensity. (a) $N = 3$ and "ν" being set equal to $\frac{\pi}{2\sqrt{3}}$ in Eq. (31). (b) $N = 6$ and $\nu = \frac{\pi}{2\sqrt{6}}$. (c) $N = 9$, $\nu = \frac{\pi}{2\sqrt{9}}$.

(b), (c) show the finesse that corresponds to the number of input waves and the half-width shrinks as the number of input waves increases. The finesses of 6 and 9 beam combiners are two and three times higher than that of a 3 beam combiner respectively.

Figure 9(a) shows the output intensity of 6 beam combiner is plotted as a function of grating strength ν for the case when all the input waves are in phase. Figure 9(b) shows the output intensity as a function of the phase angle between the adjacent waves for three different values of ν that correspond to output intensities 2, 4 and 6, as shown in Figure 9(a). The height of peak decreases as the grating strength reduces. The height of the solid line plot in Figure 9(a) is equal to the maximum intensity value. The finesses of the three peaks have the same value of 6, regardless of the grating strength.

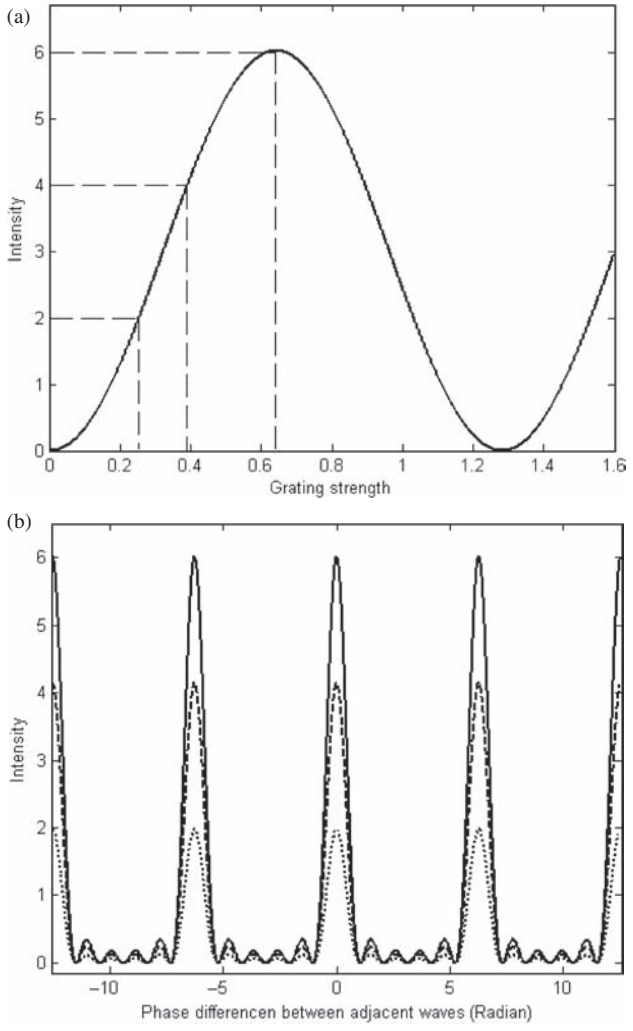

Fig. 9. (a) Simulation results showing the intensity of the output wave as a function of grating strength "ν." Six input waves have unit intensity and are considered to be in-phase i.e., ϕ is set to zero in Eq. (31). (b) Simulation result showing the intensity of the output wave as a function of phase angle between the adjacent waves plotted for three values of "ν." The solid line corresponds to $\nu = 0.6409$, the dashed line for $\nu = 0.3850$, and the dotted line for $\nu = 0.2500$ in Eq. (31).

6. EXPERIMENTAL DEMONSTRATION OF SIX-BEAM COMBINER VARYING PHASE ANGLE BETWEEN ADJACENT WAVES

Using our simulation, we first studied the intensity profile of the output wave S_0 of a six beam combiner. Figure 10 shows the result for the case when grating strength is set equal to that for holograms in the 2nd sample, 0.23π, discussed earlier. Figure 10 shows that the maximum peak height from the experiment with the 2nd sample can be expected to be 5.8.

Experimentally, we combined the six waves using the 2nd sample. Figure 11 shows the experimental set-up using a plano-convex lens that is used to demonstrate the beam combiner. The input wave from Nd-YAG laser illuminates the holograms in the direction of reference S_0 which is split into 6 waves. The waves represented by solid lines are generated in the beam splitter mode. The flat surface of the lens faces towards the hologram which acts like a point source with six split waves. Both surfaces of the lens contribute to refractions to minimize the spherical aberration. The six waves emerge parallel on the other side of the lens and are reflected by the mirror. Since the angle between the adjacent object waves is set constant via holographic recording, the phase delay between the adjacent diffracted waves ϕ is constant for a given angle of the mirror. The six reflected waves illuminate the holograms in the beam combiner mode. Combined beam is partially reflected by the beam splitter placed after the hologram. The partially reflected beam is monitored by photo detector while adjusting the mirror angle to continuously vary the phase angle difference.

The sum of the intensities of individual beams (defined as $6I_0$) is measured using an amplified photodetector whose output reads 760 mV after the splitter in Figure 11. I_0 stands for the average intensity of each individual beam.

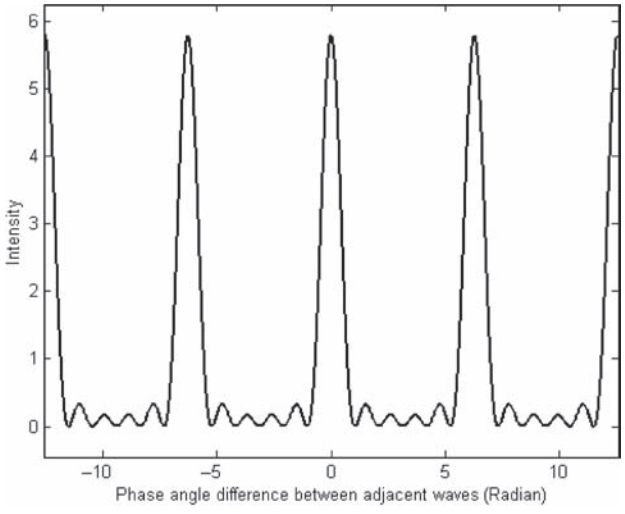

Fig. 10. The intensity of S_0 is plotted as a function of the phase angle difference between the adjacent waves for $\nu = 0.23\pi$.

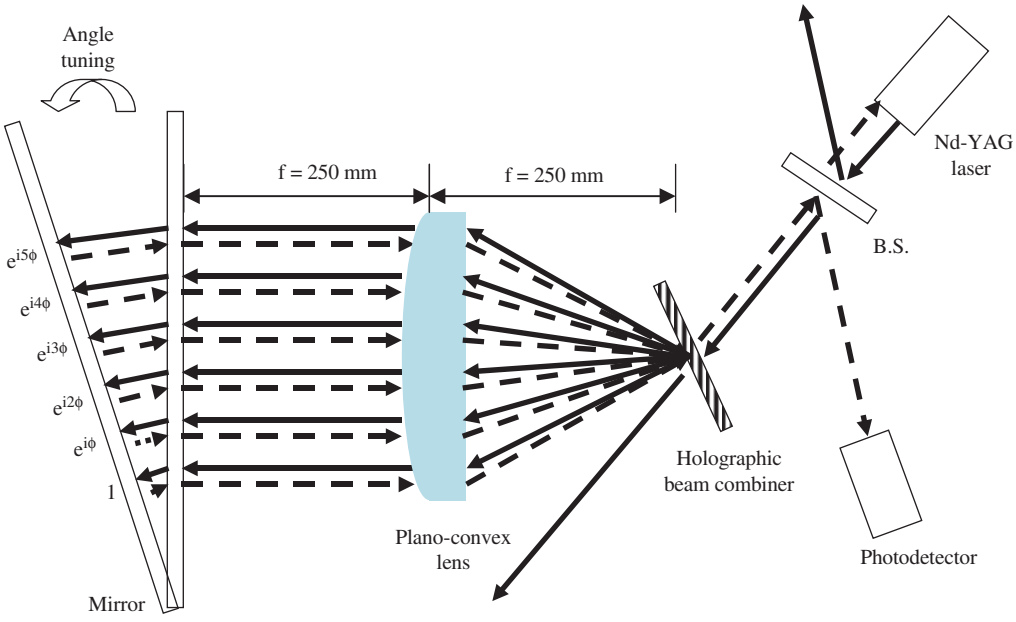

Fig. 11. Experimental setup for beam combining using the 2nd sample which has six superimposed gratings. The beam combining characteristic is investigated by varying the phase angle between the adjacent waves. The focal length of lens used in this experiment is 25 cm.

At this point, the undeflected beam was measured as 20 mV. For a ν value 0.23π, it is estimated from our theory that the maximum height of peak will correspond to a voltage 734 mV. Figure 12 shows the intensity of the partially reflected combined beam measured by the photodetector. It is noted from the 3rd and 4th peak on the left that the half width covers 0.7 fractional divisions in one rectangular box and the distance between the peaks is 4 fractional divisions. This measurement yields the finesse of six beam combiner as 5.7 which is approximately equal to the value that we estimated theoretically. The height of the highest peak is measured as 265 mV at the detector shown Figure 11. If we take into account the beam splitter reflectivity to be 61.54% and the reflection at the surface of the hologram, the intensity of the combined beam should correspond to 475.6 mV at the detector. The experimental output is still lower than the theoretically expected output of 734 mV which is attributed to residual imperfections in the experimental process and the inherent plane wave approximations in the coupled-wave theory.

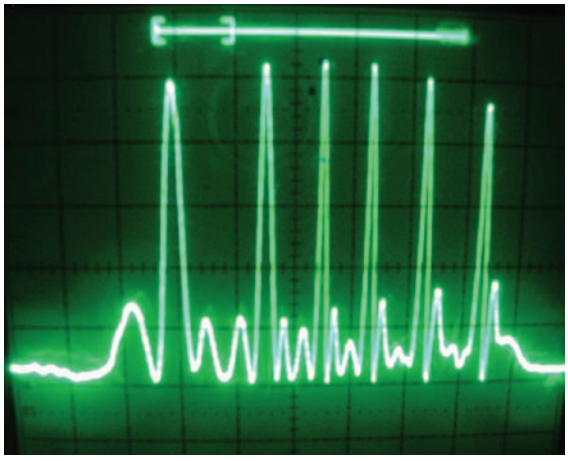

Fig. 12. An oscilloscope trace shows the intensity measured by the photodetector in the experimental setup shown Figure 11. One longitudinal division in the trace corresponds to 50 mV and the lateral division corresponds to 0.1s. The dc offset in the photodetector is ~100 mV.

Degradation of the efficiency of a holographic beam combiner can also be caused by either a cross coupled mode resulting from the double diffraction of the reconstructed wave S_0. In this case, input waves are not completely diffracted into the direction of reference wave S_0 as the reconstructed wave S_0 is partially diffracted again into the directions of the six object waves ($S_1 \sim S_6$) before leaving the holographic gratings. Also, if the input wave illuminates a location away from the center of the hologram, the grating strength (0.23π at the center of the hologram) decreases along the radius of the hologram showing the Gaussian distribution. Additionally, the error in angle displacement during holographic recording can also cause phase angle difference variation between the adjacent beams. Such difference variation can result in phase angle mismatch for the input beams that can neither be in-phase simultaneously nor being fully combined.

7. CONCLUSION

In summary, we presented numerical results using the coupled-wave theory that revealed the grating modulation strength for efficient beam combining, and predicted the effect of non-equal beam intensities and phase angle variation on the performance of a beam combiner. We also demonstrated an experimental realization of a beam

combiner using angle multiplexed holographic gratings on a thick polymeric substrate. Experimentally measured efficiency in beam combining agrees with our theoretical model.

References and Notes

1. A. Liem, J. Limpert, H. Zellmer, and A. Tünnermann, *Opt. Lett.* 28, 1537 **(2003)**.
2. Y. Jeong, J. Sahu, D. Payne, and J. Nilsson, *Opt. Exp.* 12, 6088 **(2004)**.
3. T. H. Loftus, A. Liu, P. R. Hoffman, A. M. Thomas, M. Norsen, R. Royse, and E. Honea, *Opt. Lett.* 32, 349 **(2007)**.
4. I. V. Ciapurin, L. B. Glebov, and V. I. Smirnov, *Proc. of SPIE* 5335, 116 **(2004)**.
5. M. S. Shahriar, J. Riccobono, M. Kleinschmit, and J. T. Shen, *Opt. Commun.* 220, 75 **(2003)**.
6. H. N. Yum, P. R. Hemmer, A. Heifetz, J. T. Shen, J.-K. Lee, R. Tripathi, and M. S. Shahriar, *Opt. Lett.* 30, 3012 **(2005)**.
7. L. S. Sadovnik, A. Manasson, V. A. Manasson, and V. A. Yepishin, *Proc. SPIE* 3464, 155 **(1998)**.
8. H. N. Yum, P. R. Hemmer, R. Tripathi, J. T. Shen, and M. S. Shahriar, *Opt. Lett.* 29, 1784 **(2004)**.
9. H. Kogelnik, *Bell Syst. Tech. J.* 48, 2909 **(1969)**.
10. S. K. Case, *J. Opt. Soc. Am.* 65, 724 **(1975)**.
11. R. Magnusson and T. K. Gaylord, *J. Opt. Soc. Am.* 67, 165 **(1977)**.
12. J. Zhao, P. Yeh, M. Khoshnevisan, and I. McMichael, *J. Opt. Soc. Am. B* 17, 898 **(2000)**.
13. J. Zhao, X. Shen, and Y. Xia, *Opt. & Laser Tech.* 33, 23 **(2001)**.
14. H. Kobolla, J. Schmidt, J. T. Sheridan, N. Streibl, and R. Völkel, *J. Mod. Opt.* 39, 881 **(1992)**.

Received: 4 April 2008. Accepted: 19 September 2008.